MODELLING OF WIND FLOW PATTERN AFFECTING SNOWDRIFT

PhD Thesis Synopsis

Submitted by

GANESH KUMAR

Under the supervision of

Prof. Ajay Gairola

CENTRE OF EXCELLENCE IN DISASTER MITIGATION AND MANAGEMENT

INDIAN INSTITUTE OF TECHNOLOGY ROORKEE

ROORKEE – 247 667 (INDIA)

NOVEMBER 2019

1. INTRODUCTION

The wind is a significant metrological parameter which is used in wind energy harvesting and assessment of aeolian phenomena. It transports snow from one place to another place known as snow drifting and the deposition pattern of the natural precipitated snow is changed. The snow drifting causes many problems like invisibility, snow cornice formation and blockages of highways. Due to the failure of snow cornices, the snowpack on the formation zone of an avalanche is destabilized and trigger an avalanche. The wind-driven snow on the surface is comparatively more compact and it stays for a longer period in the region. In the mountainous region, wind transport snow from windward to leeward side and excess snow deposition on the leeward formation zone trigger avalanche. Fracture initiation and propagation in snowpack are generated due to the self-weight of the snow (Mahajan et al., 2010). Seeing the contributions of wind-driven avalanche hazard, the researchers have tried to simulate and model the snowdrift using numerical methods and wind tunnel experiments. The study of wind profile and its effect on the snowdrift is beneficial for avalanche forecasting, snowdrift control and planning of protection of highways in the mountainous regions.

The logarithmic wind speed profile and various modifications to it are further used in stable stratification at inappropriately high altitudes (A. Clifton et al., 2006; Gryning et al., 2007; Kent et al., 2018). With the similarity theory based on the Monin-Obukhov concept, the profiles of wind speed and turbulence can be calculated as per Eq. 1.1 (Tennekes, 1973).

$$u(z) = \left(\frac{u_*}{\kappa}\right)\left\{ln\left(\frac{z}{z_0}\right) - \psi\left(\frac{z}{L_*}\right)\right\} \quad (1.1)$$

Where u(z) is the wind velocity at height z, roughness length z_0, Friction velocity u_*, Monin-Obukhov length L_*, stability correction ψ and Von Karman constant κ=0.4. The Monin-Obukhov theory applies restricted to the surface layer (roughly 10% of the height of the atmospheric boundary layer) (Cenedese et al., 1997).

Computational fluid dynamics technique is used to simulate the wind flow around the hill and the snowdrift control structures for mitigation of avalanche hazard in the mountainous region. The modelling of wind flow around snowdrift control structures (snow fence and Jet roof) and investigation of a new simulant material, foam beads (expanded Polystyrene) for snowdrift modelling have been carried out under the research work.

2. THE OBJECTIVES OF THE RESEARCH

The main objectives of this research were:

(i) To investigate wind flow profile around the structure

(ii) To estimate the influence zone of structures affecting snowdrift

(iii) Numerical modelling and simulation of the wind flow profile

(iv) Modelling of snow deposition pattern for designing a control structure

3. Methodology

In the present research work, an experimental setup in the snow filed area and a re-circulating wind tunnel were established to observe the wind profile for drifting phenomenon. The drifted snow-mass around the structures was analyzed to find the performance of snowdrift control structure at Banihal Top, Jammu and Kashmir, India in the Himalayan region. The wind profile around the hill was modelled using a CFD tool named ANSYS Fluent. The wind profile at the experimental site and snowdrift deposition around a snow fence were studied under the scope of research work.

3.1 Field Experiments

The field observation and data collection for the research work have been carried out at Banihal top (Jammu and Kashmir, India). Banihal Top lies at 190 Km from Jammu towards Srinagar in PirPanjal range of the Himalayas. It experiences snow precipitation in the winter season between November and April. The study area existing at the mountain ridgeline helps to observe the wind, snowdrift and avalanche activities. To mitigate and to control the avalanches from the avalanche site, different avalanche control structures (snow rake and snow bridge) and snowdrift control structures (snow fence and jet roof) have been installed at the study area (Chaudhary and Singh, 2006).

Wind sensors are installed across the ridgeline and wind speeds were measured to observe the effect of the ridgeline and the snowdrift activities. The seven wind sensors were installed to study the wind profile around the ridgeline. An acoustic-based snow flux measuring

instrument called FlowCapt was installed along with Automatic weather station at the experimental site (Fig . 1)

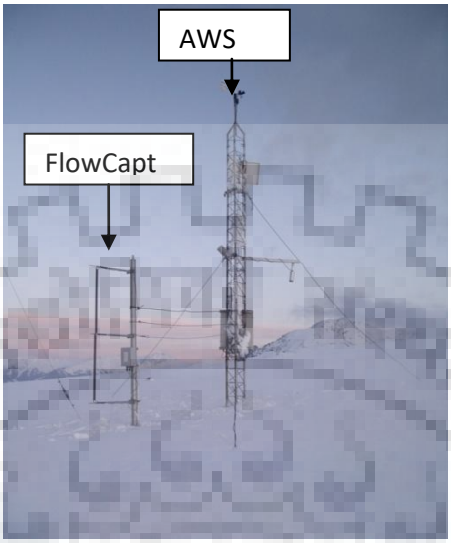

Fig. 1: FlowCapt and AWS installed at the snowfield observatory

3.2 Wind Tunnel Experiments

The experimental methods in the wind tunnel are used to simulate the snowdrift and to validate the numerical method of the transport system. Andrew James Clifton(A.J. Clifton, 2007) investigated the boundary layer conditions before and after snowdrift in a wind tunnel. He worked with natural snow and simulated the snowdrift. Sand particles movements were observed in the wind tunnel experiments by Sang Joon et.al (Lee et al., 2002). He used snow fence models of different heights and porosities to observe the sand particles movements for simulation of a snowdrift. Y. Anno (Anno, 1984a) used activated clay particles in the wind tunnel to model the snowdrift. The clay particles were suitable in respect to grain size, the angle of repose and range of cohesion in comparison to other materials used conventionally as substitutes for snow particles. He found precise similitude between the model and its prototype in modelling a snowdrift in small-scale modelling. However, any researchers have not used foam beads (expanded Polystyrene) previously. Hence, an attempt was made to simulate the snowdrift deposition pattern using foam beads in the small re-circulating wind tunnel in this thesis.

A closed re-circulating wind tunnel of 4m in length was designed and built in-house to carry out the experiments for the modelling of a snowdrift with foam beads. The whole setup

was mainly divided into three sections namely (1) horizontal, (2) inclined and (3) vertical (Fig. 2) resembling different terrain slopes for the experimental simulations. The horizontal section had the main test space for simulation study of deposition pattern and observation of foam beads transportation under the wind force. Foam beads having the spherical shape of average diameter 0.0015 m and average bulk density of 50 kg/m^3 had been used as simulants in the wind tunnel. An exhaust fan (blade diameter 0.6 m and rpm 1400 was fitted coaxially with the horizontal section to produce the wind speed up to 14 m/s for the movements of foam beads in the wind tunnel.

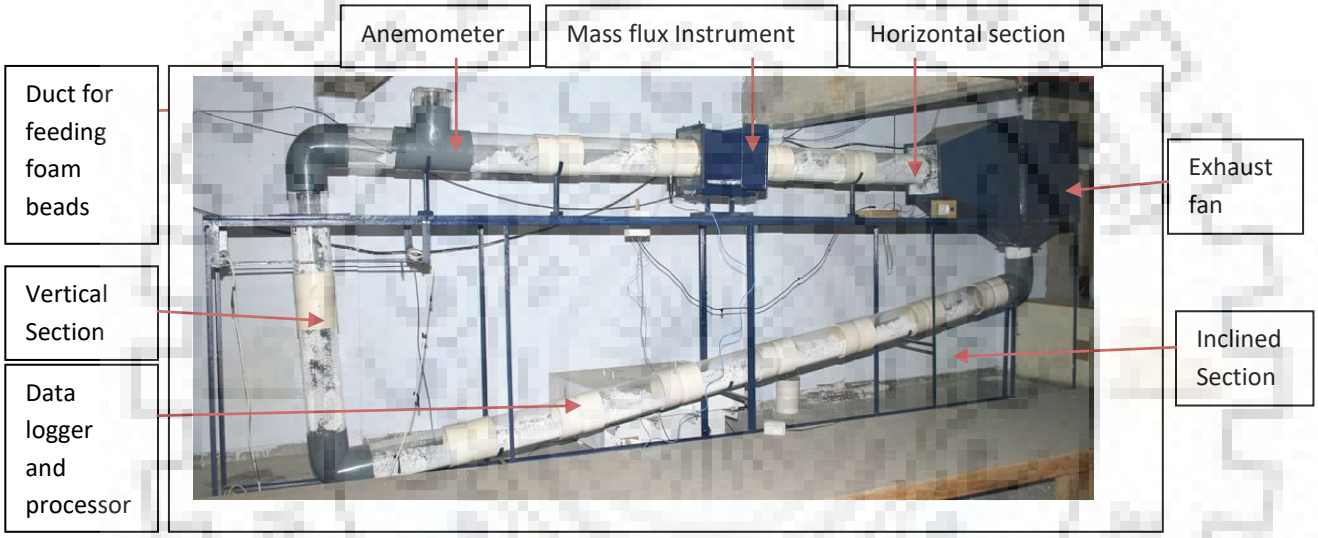

Fig. 2: A closed re-circulating wind tunnel and its different sections: (i) Horizontal, (ii) Inclined and (iii) Vertical

Snowdrift wind tunnel simulation needs to keep similarities between model and prototype in geometry, kinematics and dynamics. The study on physical modelling of snowdrift was carried out with foam beads experiments in a closed re-circulating wind tunnel. The similarities of particle density, the wind field, flow around the snow fence (structure) and dynamic similarity had been observed. These similarities are the basic requirements in the wind tunnel experiments (Zhou et al., 2014).

3.3 Numerical methods

In recent decades, a dramatic increase in computational power together with advances in computer software have allowed engineers/researchers to more accurately simulate many types

of specific cases across various engineering realms. The computational and experimental studies for wind flow over embankments or hills were introduced by Deaves (1980). Numerical method of wind flow analysis solves the Navier Stokes equations with the defined boundary conditions. Yan and Li (Yan et al., 2013) modelled wind flow over a triangular hill using four different turbulence models namely, RNG-based $k-\epsilon$ model, standard $k-\epsilon$ model, $k-\omega$ sst model and realizable $k-\epsilon$ model. The results showed that the RNG-based $k-\epsilon$ model was closest to the experimental results by Lee and Park (Lee et al., 2002) for reattachment point of wind profile on the leeward side. Kim and Patel (Kim et al., 2000) showed that the RNG based $k-\epsilon$ model gave the best results for various flow profiles and reattachment point of the separated flow region among other two-equation turbulence models. In the present paper, the RNG based $k-\epsilon$ model was used to wind flow pattern on lee side and effect of jet roof over it.

4. Results and Discussion

The experimental set up was installed at Banihal top (Jammu and Kashmir), India for meteorological and snowdrift observations. Wind flow pattern was observed on windward and leeward sides of a typical hill at the observatory. Snowdrift control structures namely snow fence and Jet roof were installed to observe their effective zones. Further computational fluid dynamics (CFD) analysis of wind flow around the structures was carried out for the wind flow modelling.

4.1 Performance of snow fence

It was observed that average wind speed at the experimental site is more than the threshold velocity for snow drifting (5 -15 m/sec) and large snowdrift activities. Snow fences (4m height) in running length of 130m were installed near the ridgeline of Pir Panjar range of Himalaya at Banihal top (Fig.-3).

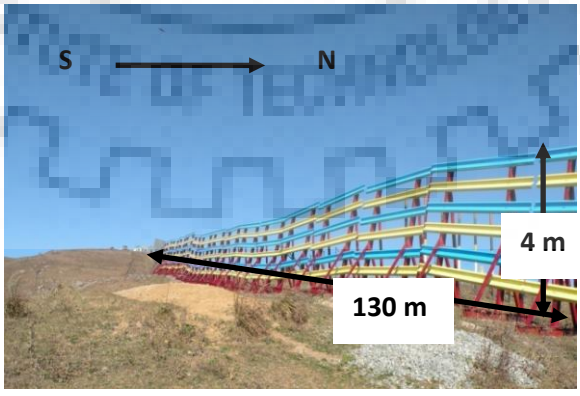

Fig.3: Snow fence installed at the experimental site (summer view)

The performance of snow fences was evaluated on the basis of snow mass deposition near the snow mass and the avalanche activities. It is observed that the deposition of drifted snow on the formation zone had reduced significantly and avalanches had not occurred from the gullies near to the snow fence.

The extension of snow deposition near the snow fence was 12 to 17 H (where H is the height of snow fence) in the leeward. It was a much lower value than extension observed by Tabler (2003). The area where the snow is deposited due to snow fence is the effective zone of snow fence. The snow deposition profile around the snow fence at the experimental site is shown in Fig. 4.

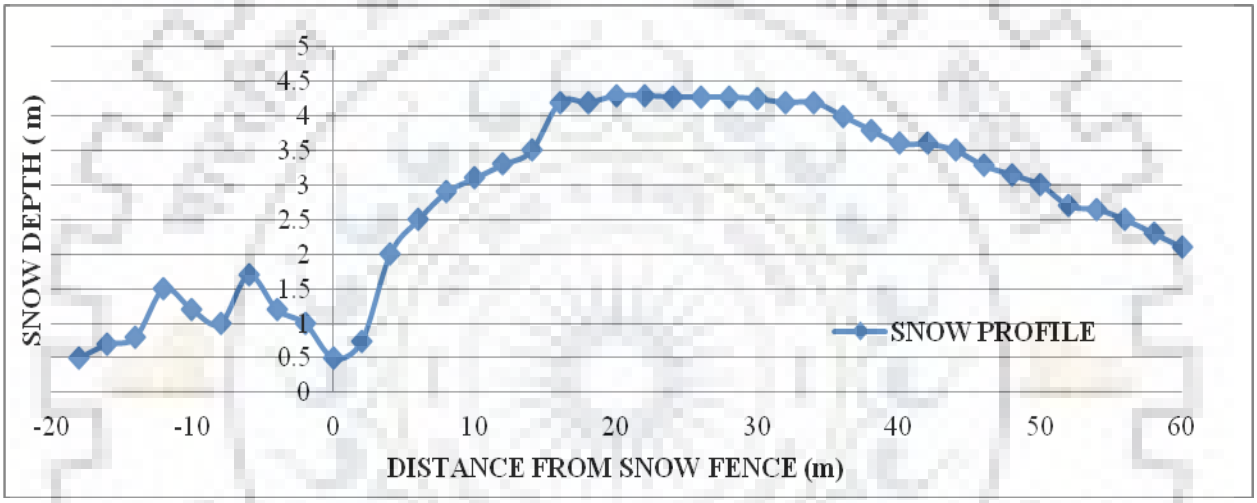

Fig. 4: Snow profile due to 4.0 m height snow fence

The low extension of drifted snow profile was due to the typical topographical feature of the experimental site, snow condition and high wind speed. The snow accumulation due to 4 m high snow fence was 120 m^3 per meter running length. The average snow accumulation per meter was 105 m^3.

4.2 Performance of Jet roof

In contrary to the function of a snow fence, a jet roof enhances the wind speed in leeward to prevent the snow deposition near to the ridgeline. The inlet cross-section area is more in comparison to exit and so it acts as a jet (David and Schaerer, 1993). Three jet roofs were installed and their effects on wind flow and snow deposition were analyzed for their performance. The jet roof was placed at the ridgeline with the smaller cross-section for airflow

near the leeward slope. Due to reverse flow snow is accumulated on leeward to form a cornice. The jet roof is used to mitigate the snow cornice formation (Fig. 5).

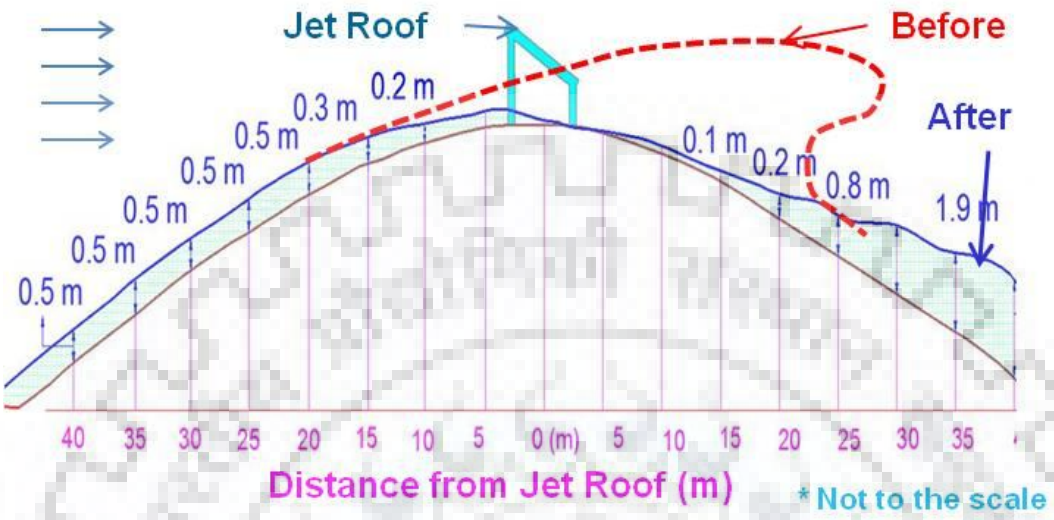

Fig. 5: Effect of the jet roof on snowdrift in the field

The reduction in cross-section results in an increase in velocity on the leeward side which opposes the reversed flow. Velocity contours for the simulation of wind flow without and with jet roof show a significant increase in the horizontal velocity along the leeward slope (Fig. 6). The velocity vectors in the reversed flow were forced in the opposite direction along the lee slope which pushes the region of reversed flow at a certain height. The modified wind flow due to jet roof mitigates snow deposition near the ridgeline on the leeward side.

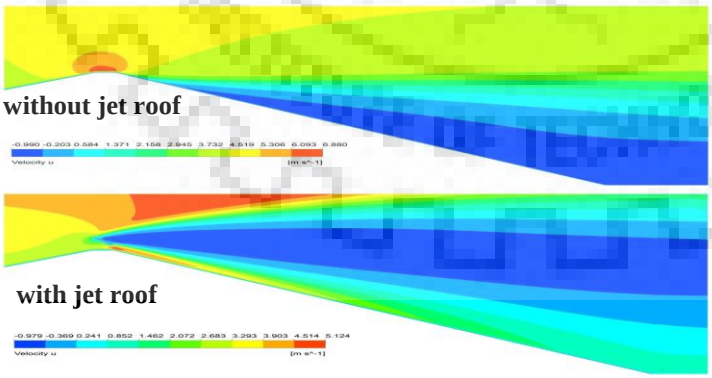

Fig. 6: Comparison of velocity contours without and with jet roof

4.3 Modelling of wind flow around the hill

The RNG based $k-\epsilon$ model is used to wind flow pattern around the hill. The atmospheric boundary layer (ABL) of the wind flow was modelled over the 2D hill model. Yang et al. (2009) established the relations of the inflow boundary conditions for a neutrally stable atmospheric boundary layer. A 2D computational domain having dimensions 10Hx30H where H is the height of the hill model was considered to study the wind flow over a scaled downhill model (1:5) (Fig. 7). Standard wall functions were applied at the boundary walls. Grid-independent test was conducted using four different mesh cases namely GT0, GT1, GT2 and GT3 (Table 2).

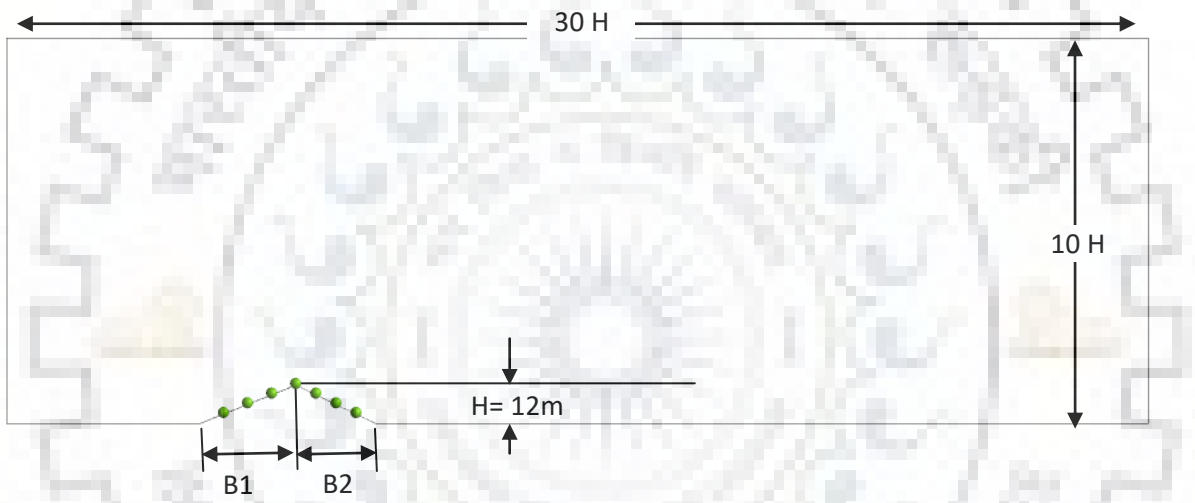

Fig. 7: Computational Domain of 2D Hill model

Table 2: Meshing parameters for grid-independent test

Mesh case / Mesh parameters	GT0	GT1	GT2	GT3
Elements	58000	116000	412000	715000
Nodes	58681	116781	413431	716931
Min. Orthogonal Quality	0.90153	0.90153	0.90157	0.90153
Max. Aspect Ratio	14.36	8.183	3.3656	5.5465

On comparing the velocity contours of the four meshes, it was found that GT2 and GT3 captured the fully developed separation zone in leeward of hill model (Fig. 8) and out of these two meshes; GT2 had better maximum aspect ratio and minimum orthogonal quality. Further, the grid-independent test was verified with the field data observed at the experimental site (Fig. 9). Hence, the simulation of wind flow was carried out on the model with mesh element numbers equal to or more than 412000.

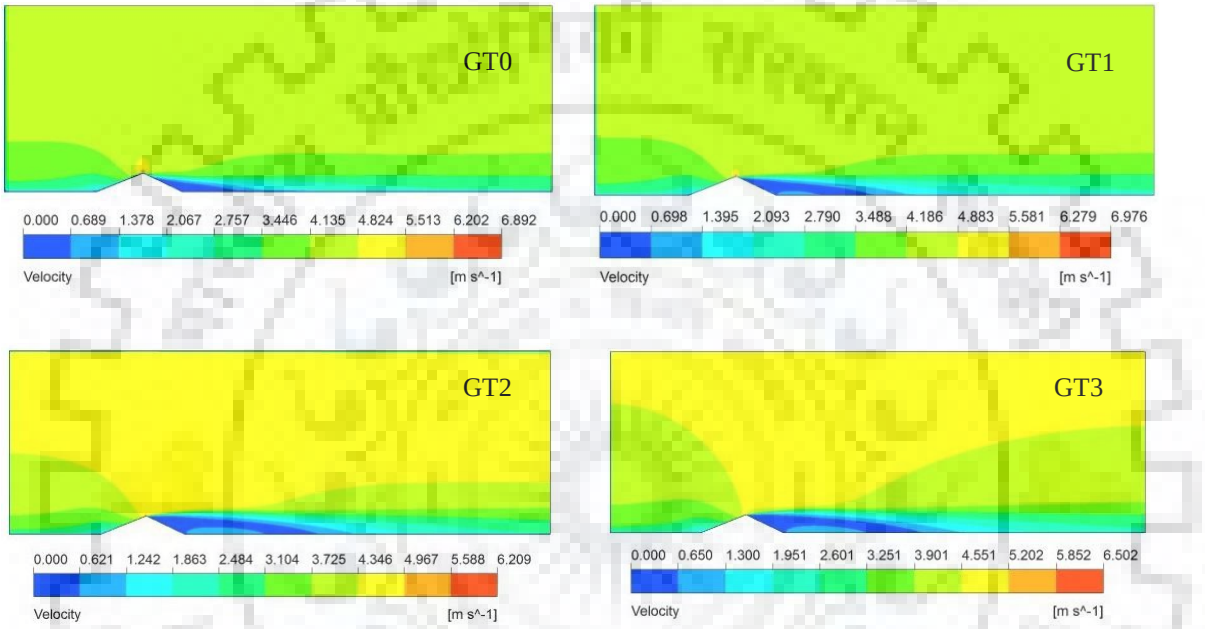

Fig. 8: Velocity contours for the mesh model GT0, GT1, GT2 and GT3

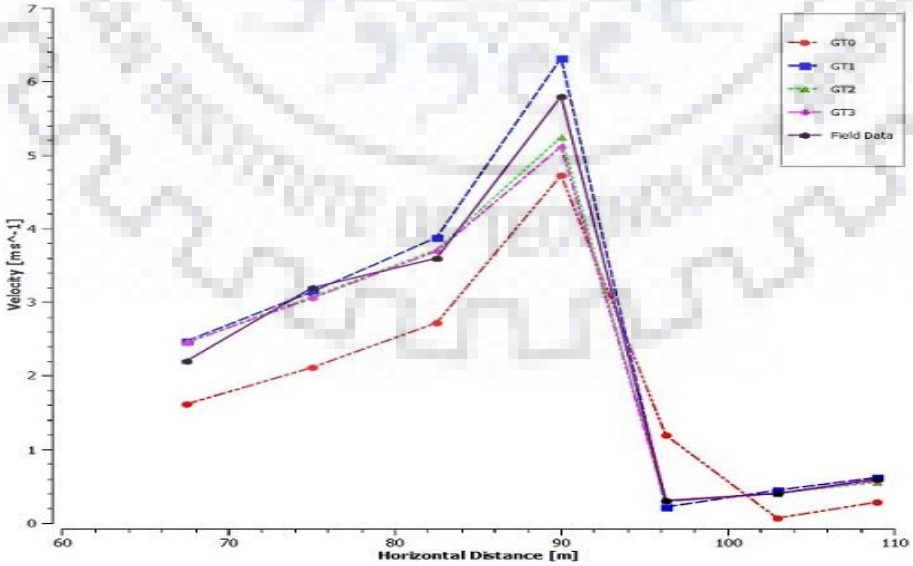

Fig. 9: Velocity comparison for seven data points

The different CFD 2D hill models were created by varying the leeward slopes and keeping the same windward slope of the experimental site. The detailed configurations of hill model slopes are illustrated in Table 3. The effect of the jet roof was observed on the experimental hill model called Banihal Top.

Table 3: Lee slopes of the Hill Models

Sr. No.	2D Model Name	Windward Base Length (B1)	Leeward Base Length (B2)	Model Hill Height (H)	Slope	Leeward Slope Angle
1	Banihal Top	30m	25m	H= 12m	1:2.08	25.64°
2	Hill12	30m	2 H= 24m	H= 12m	1:2	26.56°
3	Hill13	30m	3 H= 36m	H= 12m	1:3	18.43°
4	Hill14	30m	4 H= 48m	H= 12m	1:4	14.04°
5	Hill15	30m	5 H= 60m	H= 12m	1:5	11.31°
6	Hill16	30m	6 H= 72m	H= 12m	1:6	9.46°

The speedup ratio (Eq. 4.1) for the computational model was plotted against the dimensionless height z/H and compared with the speed up ratio for the theoretical logarithmic wind profile given at the inlet (Eq. 1.1)

$$Speed\ up\ ratio = \frac{u}{u_\infty} \tag{4.1}$$

where, u is the horizontal velocity and u_∞ is the free stream velocity. The simulated results of speedup ratio and turbulence kinetic energy are found to be similar of the theoretical profile Fig. 10 and Fig.11 respectively.

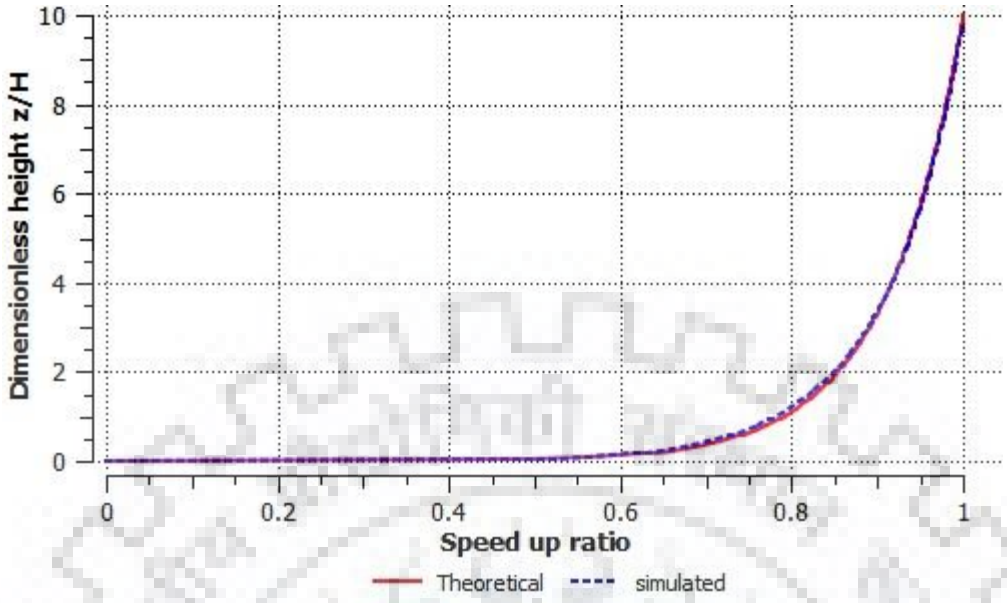

Fig. 10: Comparison of Speed up ratio

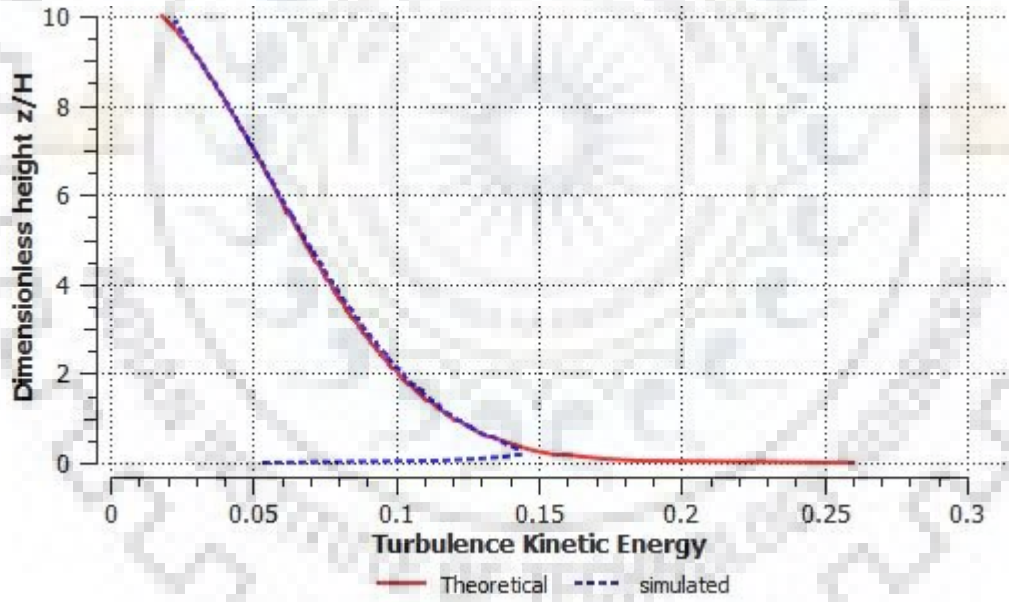

Fig. 11: Comparison of Turbulence Kinetic Energy

It was observed that the velocity was increasing upward till the peak of the hill in the windward side but there was a sudden drop in wind speed at the peak of the hill. Effect of windward slope on the flow in the leeward side was also examined by comparing the horizontal velocity at the observation height of 3m (AWS height) for hill model of Banihal Top and one with the

windward slope of 1:4. It was observed that the variation in the windward slope did not bring any significant change in the wind flow in the leeward (Fig 12).

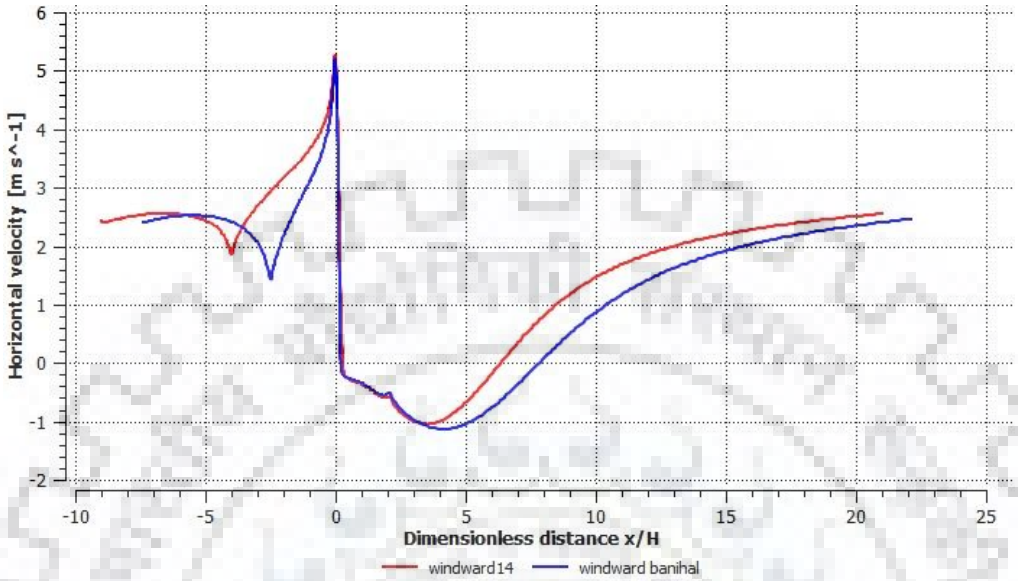

Fig. 12: Comparison of Horizontal velocity for varying the windward slope

Horizontal velocity at the observation height of 3m for the hill models (Fig. 13) show the separation point to shift downhill for hill13 in comparison to hill12. For hill14 to hill16 separation doesn't take place however point of minimum velocity shifts towards higher dimensionless distance x/H.

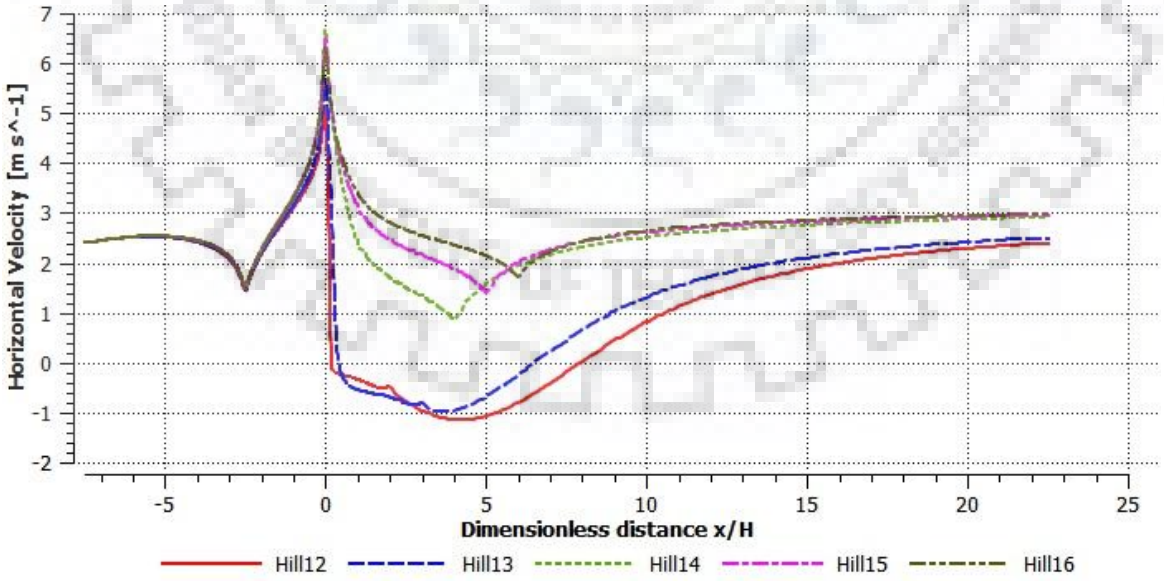

Fig. 13: Horizontal velocities at observation height for varying lee slopes

4.4 Wind Tunnel experiments

Wind tunnel test, due to its accessibility for easy control and systematic study, is regarded as an important research method. Snowdrift wind tunnel simulation requires geometric, kinematic and dynamic similarities to be established between model and prototype. The study on physical modelling of snowdrift was carried out with foam beads in a closed re-circulating wind tunnel. The similarities of particle density, the wind field and flow around the snow fence (structure) had been observed. These similarities are the basic requirements in wind tunnel experiments (Zhou et al., 2014). The similarity characteristics between snow (prototype) and foam beads (model) are illustrated in Table-1.

Table 1: Similarity characteristics of prototype and model

Ser. No.	**Type**	**Similarity Parameter**	**Prototype**	**Model**
1.	Particles	(A) Particle Dia., D (x10^{-3} m)	0.15-2.0	1.5
		(B) Particle Density, ρ_p (kg/m^3)	50-700	100
		(C) Bulk Density, ρ (kg/m^3)	18-420	50
		(D) Threshold Shear Velocity, U_{*t} (m/s)	0.15-0.36	0.25
2.	Snow Fence	(A) Height, H(m)	4	0.08
		(B) Porosity (%)	50	50
		(C) Width, B (m)	4	0.08

The similarity parameters of prototype snowdrift and model foam bead flow were analyzed and have been illustrated in Table-2.

Table-2: Similarity parameters of snowdrift (prototype) and foam bead flow (model) in the wind tunnel

Description	Physical Meaning	Similarity parameters	Snowdrift (Prototype)	Foam Bead flow (Model)
Similarity of the wind field	Aerodynamic roughness height of saltating particles	$\frac{\rho U_*^2}{\rho_p l g}$	1.34e-6 – 1.873e-5	9.56e-4
	Roughness-height Reynolds number	$\left(\frac{U_{*t}^3}{2gv}\right)_m \geq 30$	-	54
Similarity of the ejection process	Froude number of particle trajectory in the ejection process	$\frac{\rho U_{*t}^2}{(\rho_P - \rho) g d_p}$	0.004-2.166	0.05
	Similarity parameter of wind velocity	$\frac{U_{(H)}}{U_{*t}}$	29.94-71.867	36.4
Similarity of particle trajectory	Velocity at maximum structure height (m/s)	$U_{(H)}$	10.78	9.1
	Froude Number of particle trajectory in the saltation process	$\frac{\rho_P U_{(H)}^2}{(\rho_P - \rho) g l}$	3.034	106.79
	Settling velocity of the particles (m/s)	w_f	0.2-0.5	0.4
	Ratio of drag force and inertial force	$\frac{w_f}{U_{(H)}}$	0.018-0.046	0.044
Similarity of Deposition	Angle of Repose (°)	θ	35-80	38

The atmospheric boundary layer condition of turbulent flow is defined by the logarithmic wind profile. The logarithmic wind profile at the height z is given by Eq 4.2 (A. Clifton et al., 2006)

$$U(z) = \frac{U_*}{\kappa} \ln\left(\frac{z}{z_0}\right) \tag{4.2}$$

where U_* is the shear velocity, $\kappa = 0.41$ is called the Von Karman Constant and z_0 is the roughness height. The value of z_0 depends on the geometry of the snow surface. In the present paper, the value of z_0 is 0.0015 m which lies in the range of its value (0.0001 m to 0.005m) (A. Clifton et al., 2006; Holmes, 2007; Lehning et al., 2002). The value of U_* for the field is 0.56 m/s. It was found that the wind velocity pattern in the wind tunnel closely followed the logarithmic wind velocity pattern of the atmospheric boundary layer in the field (Fig.14).

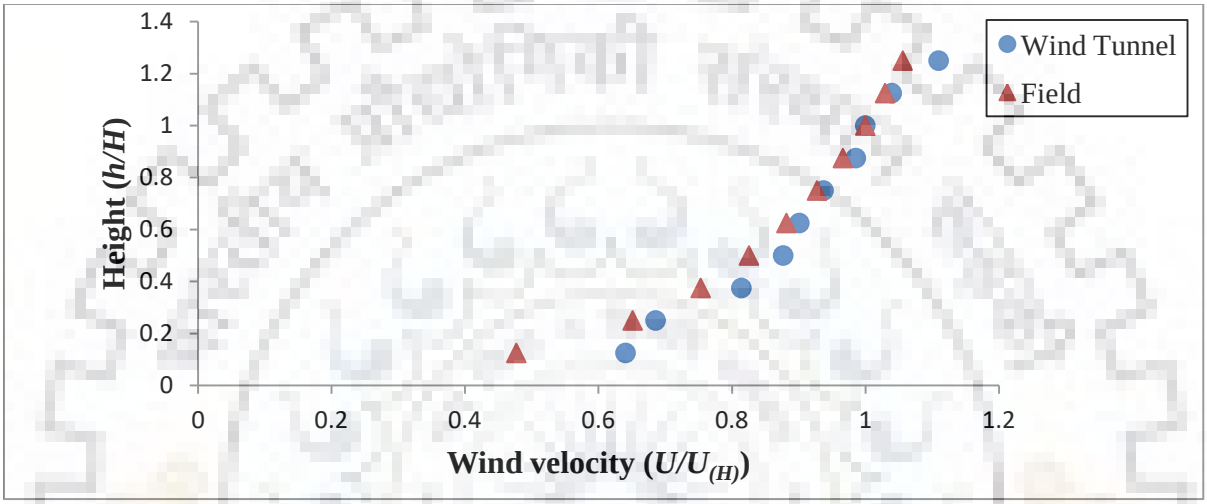

Fig. 14: Variation of dimensionless wind velocity with the dimensionless height

The turbulent kinetic energy $k(z)$ at height z for the atmospheric boundary layer is given by Eq 4.3 (Yang et al., 2009)

$$k(z) = \sqrt{c_1 \, ln(z + z_0) + c_2} \tag{4.3}$$

where the constants $c_1 = -0.6035$ and $c_2 = 1.7934$ for shear velocity $U_* = 0.511$ m/s for the atmospheric boundary layer. Zhou et. al. (2016) (Zhou, Qiang, Peng, et al., 2016) considered the value of $c_1 = -0.064$ and $c_2 = 0.588$ for $U_* = 0.35$ m/s for the wind tunnel. The values of U_* for the field and the wind tunnel are 0.56 m/s and 0.35 m/s respectively in the present paper. The constants of the turbulent kinetic energy are found statistically and so same values of constants were used in the present paper due to relatively close values of U_* for the field and the wind tunnel. The relation between the dimensionless turbulent kinetic energy (k/k_H) and dimensionless height is depicted in Fig 8. It is found that the turbulent kinetic energy (k/k_H) for the field and the wind tunnel at *h/H* greater than 0.75 are very close (Fig.15).

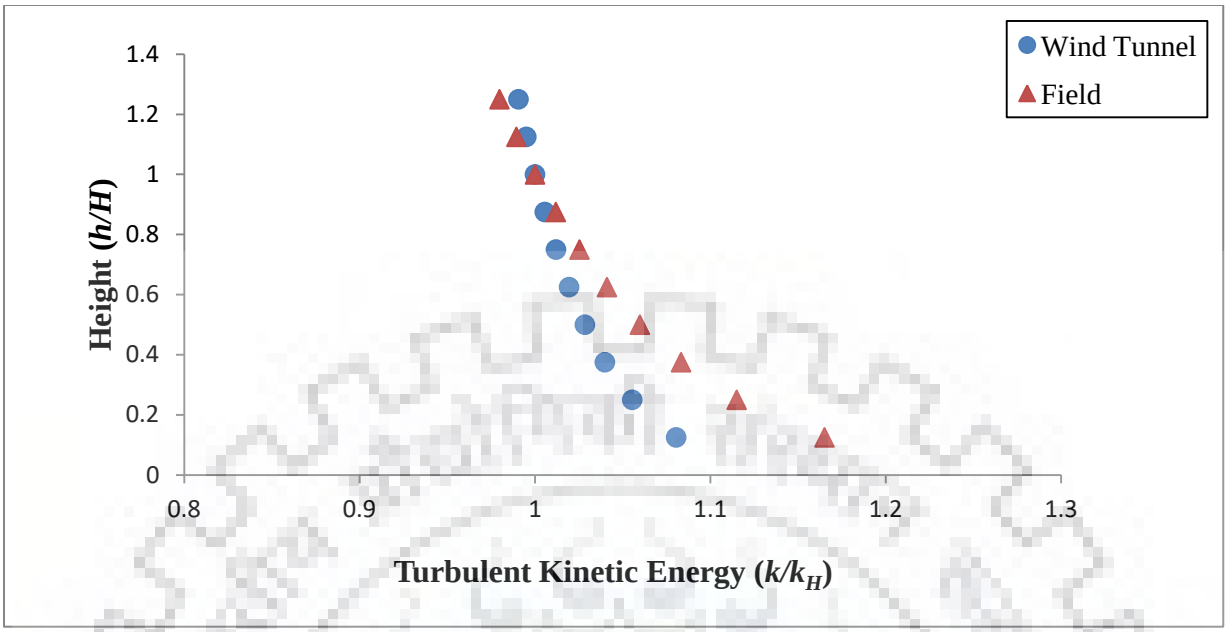

Fig. 15: Variation of dimensionless turbulent kinetic energy with the dimensionless height

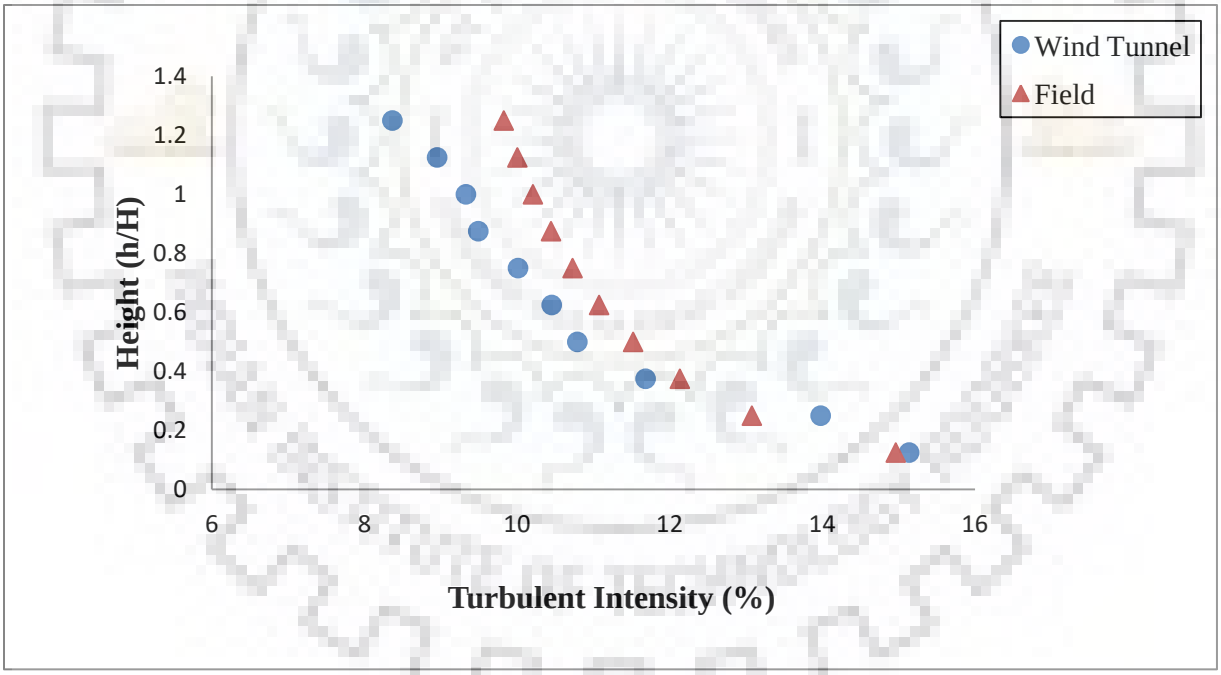

Fig. 16: Variation of turbulence intensity with the dimensionless height

The turbulent intensity $I(z)$ is obtained with the wind velocity and turbulent kinetic energy using Eq. 4.4

$$I(z) = \frac{0.913}{U(z)}\sqrt{k(z)} \tag{4.4}$$

It was found that the turbulence intensities are 10.7% and 10.0 % at the height of AWS (h/H = 0.75) and at h/H = 0.75 in the wind tunnel respectively (Fig. 16). Thus, the turbulence characteristics for the field and the wind tunnel are consistent.

4.3 Mass flux of particles

The snow mass flux was measured with FlowCapt in the snowfield. A sample of mass flux with wind speed is shown in Fig. 17. The drifting of snow was observed above the wind speed of 7 m/s. The mass flux rate varies with the surface condition and the wind speed in the field. The maximum snow flux rate of 31.2 $x10^{-3}$ $kgm^{-2}s^{-1}$ is observed at 18 m/s wind speed with the FlowCapt.

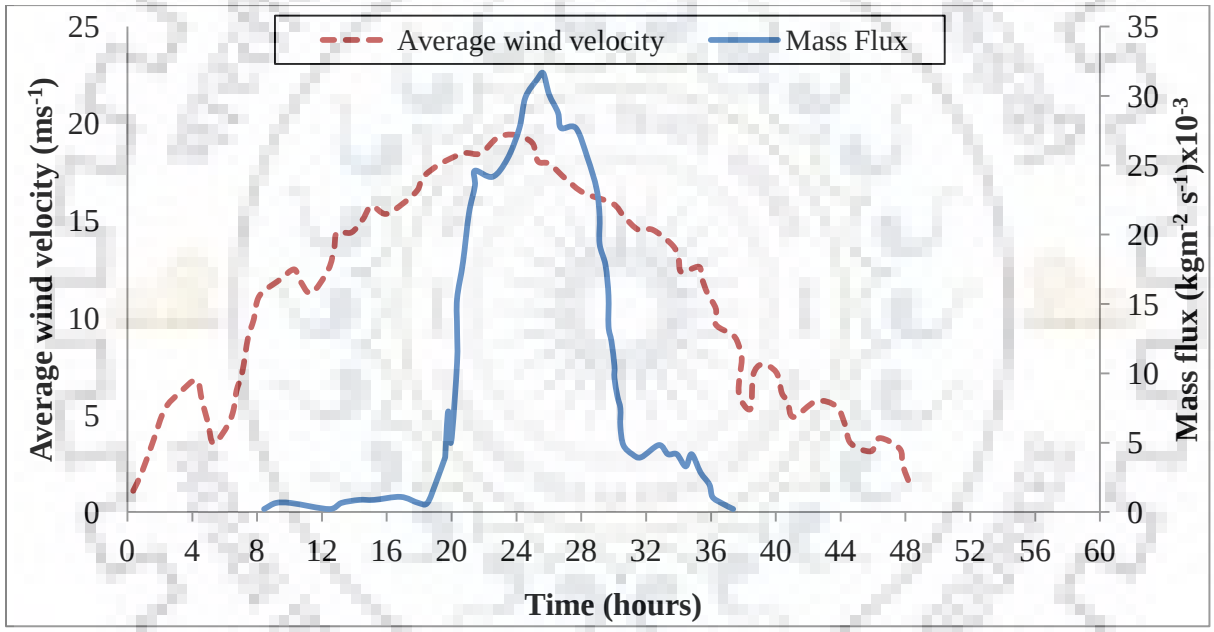

Fig. 17: Snow mass flux measured with FlowCapt and average wind speed e

The mass flux rate of snow particles and foam beads were observed with respect to the wind velocity (Fig. 18). The mass fluxes of snow and foam beads were proportional to the cubic of wind speed with a coefficient of determination (R^2) in order of 0.9. It is in line with the Bagnold's observation for the mass flux rate of sand (Bagnold, 1941). It was observed that the trend line of mass flux rate of foam beads and that of snow are parallel for the low wind speed.

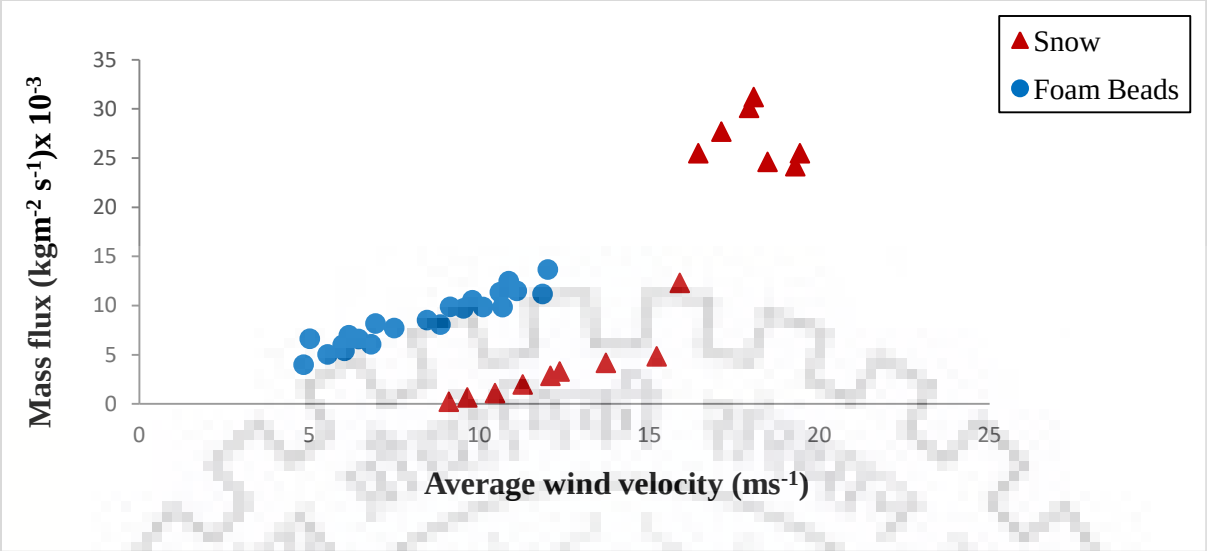

Fig. 18: Mass flux variation with wind speed

The abrupt change in mass flux rate of snow results from the fact that the large-sized particles are also drifted at the higher wind speed (more than 15 m/s).

5. Conclusion

Wind flow modelling is important for the investigation of wind energy and the prediction of aeolian phenomenon like snowdrift. Wind flow around the hill ridgeline and around the snowdrift control structures have been carried out. The snow cornice formation was majorly due to the separated wind flow on the leeward side. Their performance analysis showed that they are effective to influence the wind flow pattern in leeward side. Snow deposition depends on the height and porosity of the snow fence and it is extended up to 17 H (where H is the height of the snow fence). Due to jet roof, the velocity vectors aligned the terrain downward and reverse flow reduced to mitigate the snow cornice. The modelling of drifting snow has been attempted using the numerical method and experimental technique in the wind tunnel to solve the problems of snow cornice formation, blockage of highways due to snowdrift and avalanche hazards. Authors used the foam beads (Expanded Polystyrene) as a simulant material in the re-circulating closed wind tunnel for the snowdrift modelling as it has low density (50 kgm^{-3}) like freshly precipitated snow and is economically available. Geometric, kinematic and dynamic similarity parameters for the particles and wind field were determined to carry out wind tunnel experiments with foam beads. Turbulent kinetic energy and turbulence intensity measured at AWS height resembled the values at the corresponding height by similitude inside the test section.

REFERENCES

Anno, Y. (1984a), "Modeling of a Snowdrift Formed Around a Snow Fence by Means of Activated Clay Particles"*Journal of Agricultural Meteorology*, **40**(3), 251–255.

Anno, Y. (1984b), "Requirements for modeling of a snowdrift"*Cold Regions Science and Technology*, **8**(3), 241–252.

Bagnold, R.A. (1941), *The Physics of Blown Sand and Desert Dunes*. London : Chapman and Hall.

Cenedese, A., Cosemans, G., Erbrink, H. and Stubi, R. (1997), *Vertical profiles of wind, temperature and turbulenceHarmonisation of the pre-processing of meteorological data for atmospheric dispersion models, COST action* (Vol. COST action).

Chaudhary, V. and Singh, G. (2006), "Structural measures for controlling avalanches in formation zone"*Defence Science Journal*, **56**(5), 791–799. https://doi.org/10.14429/dsj.56.1947

Clifton, A., Rüedi, J.D. and Lehning, M. (2006), "Snow saltation threshold measurements in a drifting-snow wind tunnel"*Journal of Glaciology*, **52**(179), 585–596. https://doi.org/10.3189/172756506781828430

Clifton, A.J. (2007), *Wind Tunnel Investigations of Boundary Layer Conditions Before and During Snow Drift*. https://doi.org/https://doi.org/10.3929/ethz-a-005420531 Rights

David, M. and Schaerer, P. (1993), *Avalanche handbook* (Vol. 18). The Mountaineers 1001 SW Klickitat Way, Suite 201 Seattle, Washington 98134. https://doi.org/10.1016/0148-9062(77)90015-8

Deaves, D.M. (1980), "Computations of wind flow over two-dimensional hills and embankments"*Journal of Wind Engineering and Industrial Aerodynamics*, **6**(1–2), 89–111. https://doi.org/10.1016/0167-6105(80)90024-0

Gryning, S.E., Batchvarova, E., Brümmer, B., Jørgensen, H. and Larsen, S. (2007), "On the extension of the wind profile over homogeneous terrain beyond the surface boundary layer"*Boundary-Layer Meteorology*, **124**(2), 251–268. https://doi.org/10.1007/s10546-007-9166-9

Holmes, J.D. (2007), *Wind Loading of Structures* (Second). Taylor and Francis, London.

Kent, C.W., Grimmond, C.S.B., Gatey, D. and Barlow, J.F. (2018), "Assessing methods to extrapolate the vertical wind-speed profile from surface observations in a city centre during strong winds"*Journal of Wind Engineering and Industrial Aerodynamics*, **173**(April 2017), 100–111. https://doi.org/10.1016/j.jweia.2017.09.007

Kim, H.G., Patel, V.C. and Lee, C.M. (2000), "Numerical simulation of wind flow over hilly terrain"*Journal of Wind Engineering and Industrial Aerodynamics*, **87**(1), 45–60. https://doi.org/10.1016/S0167-6105(00)00014-3

Lee, S.J., Park, K.C. and Park, C.W. (2002), "Wind tunnel observations about the shelter effect of porous fences on the sand particle movements"*Atmospheric Environment*, **36**(9), 1453–1463. https://doi.org/10.1016/S1352-2310(01)00578-7

Lehning, M., Naaim, F., Naaim, M., Brabec, B., Doorschot, J., Durand, Y., … Zimmerli, M. (2002), "Snow drift: Acoustic sensors for avalanche warning and research"*Natural Hazards and Earth System Sciences*, **2**(3–4), 121–128. https://doi.org/10.5194/nhess-2-121-2002

Mahajan, P., Kalakuntla, R. and Chandel, C. (2010), "Numerical simulation of failure in a layered thin snowpack under skier load"*Annals of Glaciology*, **51**(54), 169–175. https://doi.org/10.3189/172756410791386436

Tabler, R.D. (2003), "Controlling blowing and drifting snow with snow fences and road design, NCHRP Project 20-7(147)"*National Cooperative Highway Research Program Transportation Research Board of the National Academies*, (August), 346.

Tennekes, H. (1973), *The Logarithmic Wind ProfileJournal of the Atmospheric Sciences* (Vol. 30). https://doi.org/10.1175/1520-0469(1973)030<0234:TLWP>2.0.CO;2

Weerasuriya, A.U. (2013), "Computational Fluid Dynamic (CFD) Simulation of Flow around Tall Buildings"*Engineer: Journal of the Institution of Engineers, Sri Lanka*, **46**(3), 43–54. https://doi.org/10.4038/engineer.v46i3.6784

Yan, B.W., Li, Q.S., He, Y.C. and Chan, P.W. (2013), "Numerical simulation of topographic effects on wind flow fields over complex terrain"In *Asia-Pacific Conferenceon Wind Engineering* (pp. 541–550). https://doi.org/10.3850/978-981-07-8012-8

Yang, Y., Gu, M., Chen, S. and Jin, X. (2009), "New inflow boundary conditions for modelling the neutral equilibrium atmospheric boundary layer in computational wind engineering"*Journal of Wind Engineering and Industrial Aerodynamics*, **97**(2), 88–95. https://doi.org/10.1016/j.jweia.2008.12.001

Zhou, X., Hu, J. and Gu, M. (2014), "Wind tunnel test of snow loads on a stepped flat roof using different granular materials", 1629–1648. https://doi.org/10.1007/s11069-014-1296-z

Zhou, X., Kang, L., Gu, M., Qiu, L. and Hu, J. (2016), "Numerical simulation and wind tunnel test for redistribution of snow on a flat roof"*Jnl. of Wind Engineering and Industrial Aerodynamics*, **153**(June), 92–105. https://doi.org/10.1016/j.jweia.2016.03.008

Zhou, X., Kang, L., Yuan, X. and Gu, M. (2016), "Wind tunnel test of snow redistribution on flat roofs"*Cold Regions Science and Technology*, **127**(May), 49–56. https://doi.org/10.1016/j.coldregions.2016.04.006

Zhou, X., Qiang, S., Peng, Y. and Gu, M. (2016), "Wind tunnel test on responses of a lightweight roof structure under joint action of wind and snow loads"*Cold Regions Science and Technology*, **132**, 19–32. https://doi.org/10.1016/j.coldregions.2016.09.011